Process optimization and revamping of combined-cycle heat and power plants integrated with thermal desalination processes

Juan I. Manassaldi[1], Miguel C. Mussati[1,2], Nicolás J. Scenna[1], Tatiana Morosuk[3], Sergio F. Mussati[1,2,*]

[1] CAIMI (UTN Facultad Regional Rosario), Zeballos 1346, S2000BQA, Rosario, Argentina

[2] INGAR Instituto de Desarrollo y Diseño (CONICET-UTN), Avellaneda 3657, 3000, Santa Fe, Argentina

[3] Institute for Energy Engineering, Technische Universität Berlin, Marchstr. 18, 10587 Berlin, Germany

Keywords: dual-purpose desalination plant, three pressure HRSG, multi-stage flash desalination, superstructure, MINLP mathematical model

Abstract

Optimal revamping, sizing, and operation of an existing gas-turbine combined-cycle dual-purpose power/desalination plant – simultaneous electricity and freshwater generation – which operates with a heat recovery steam generation with one-pressure level (1P-HRSG) and a multi-stage flash desalination process, is addressed. The sizes and configurations of the gas turbine and desalination unit are kept the same as in the existing plant through the study. However, the 1P-HRSG is conveniently extended to two- or three-pressure levels with different exchanger arrangements, including steam reheating. To this end, a superstructure-based representation of the HRSG simultaneously embedding several candidate structures was proposed and a mixed-integer nonlinear programming model was derived from it.

One revamping case consisted in maximizing the ratio between the freshwater production rate and the heat transfer area of HRSG, keeping unchanged the electricity generation rate (around 73 MW). It was found that the inclusion of a 3P-HRSG resulted in an increase of 13.782 $kg \cdot s^{-1}$ in the freshwater production, requiring 22753 m^2 of heat transfer area less in the HRSG. Another revamping case consisted in maximizing the profit, contemplating the possibility to sell extra amounts of electricity and freshwater. Sale prices, for which producing extra electricity and freshwater is beneficial, were determined.

1 Introduction

The demands of energy and water have considerably increased over the last decades as a consequence of mainly the growth of population and limitations in fuel and freshwater resources. The cogeneration of water and power by integrating combined gas/steam power generation cycles with thermal seawater

desalination (TSD) plants turns into an auspicious alternative for a cleaner production of both electricity and freshwater. As the heat recovery steam generator (HRSG) produces steam using the exhaust gases leaving the gas turbine (GT), they play a key role in the combined-cycle heat and power (CCHP) plants because its configuration, design, and operating mode considerably affect the overall efficiency of the integrated process. (In this paper, the terms “configuration” and “structure” are used as synonymous).

There are several papers addressing the study of coupled CCHP plants and thermal desalination systems – dual-purpose power/desalination plants (DPDP) – considering different types of cycles including organic Rankine cycles (ORC) [1,2], CO_2 cycles [3,4], and water Rankine cycles [5-11]. The case studies differ in the considered process structures, optimization methodologies, and optimization criteria.

Baccioli et al. [1] compared two fixed-structure waste heat recovery systems integrating an oil and ORC circuits with a multi-effect distillation (MED) desalination plant for simultaneous electricity generation and freshwater (distillate) production. The former consisted of a cascade configuration where the heat load required in the MED system is supplied by the condensation heat from the ORC. The second one consisted of a hybrid serial cascade where the condensation heat of the ORC is used to preheat the feed of the MED system and the heat condensation of the oil circuit is used in the MED first effect for seawater evaporation. The authors modeled each fixed configurations in Aspen HYSYS. For same input data, the simulation results showed that the highest profitability index is obtained with the serial-cascade configuration.

Recently, Alharbi et al. [3] presented an exergoeconomic analysis and optimization of a fixed-structure integrated system of a supercritical CO_2 Brayton cycle with a MED system. By using a genetic algorithm (GA) supported in Engineering Equation Solver (EES) software, single-objective optimization runs were performed to find the optimal design considering three objective functions: energy utilization factor, exergy efficiency, and total product unit cost. Also, multi-objective optimizations were performed by considering the three mentioned criteria. The authors highlighted the preference of multi-objective optimal designs instead of single-objective designs.

By using Aspen PLUS, Luo et al. [5] analyzed and compared a dual-purpose system consisting of a chemically recuperated gas-turbine (CRGT) cycle and a TSD plant. They simulated and compared five fixed-structure processes: the mentioned CRGT/MED system, a boiler/steam turbine (ST)/MED system, a boiler/ST/multi-stage flash (MSF) desalination system, a combined cycle (CC)/MED system, and a CC/MSF. The CRGT/MED configuration resulted in the lowest values of costs of electricity and freshwater.

Gadhamshetty et al. [6] proposed a fixed-structure integrated system consisting of a combined-cycle power plant (CCPP) that includes an air-cooled condenser (ACC), a thermal energy storage (TES) tank, an absorption refrigeration system (ARS), and a MED plant. The heating requirements in the ARS and MED systems are supplied by the waste heat from CCPP while the cooling requirements in

the ACC and MED systems are satisfied by the TES chilled water. The EES software was used to model the CCPP and ARS systems and MATLAB to model the TES system. The authors highlighted the advantage of using the TES system to improve the ACC performance, mainly at high ambient temperatures.

Rensonnet et al. [8] focused on simulation and thermoeconomic analysis of different configurations considering GT and reverse osmosis (RO), CC and RO, CC and MED. Also, hybrid systems by combining CC/MED/RO in different ways were investigated. To study each configuration, the authors used the Structural Theory of Thermoeconomics [12], which is based on the Theory of Exergetic Cost [13].

Ahmadi et al. [9] performed energy, exergy, and exergoeconomic analyses of a fixed-structure DPDP consisting of a 40 MW GT power plant and a MED desalination system with thermal vapor compression (TVC). By using a GA, the authors performed multi-objective optimizations considering the total exergy destruction rate, unit electricity price, total cost rate, gain output ratio, distilled water cost, and total exergy efficiency.

Wu et al. [10] proposed a mixed-integer nonlinear programming (MINLP) model to optimize the integration of a MSF desalination system, or a RO system, or a MSF/RO hybrid process with a boiler with a condensation-extraction ST or a back-pressure ST. Integer variables were used to model the number of stages in the MSF system and Boolean variables to select the ST type (condensing-extraction or back-pressure ST) and the desalination system (MSF, RO, or hybrid MSF/RO systems). The mass flowrates, pressures, and concentrations of streams and heat transfer areas were considered as real (continuous) variables. They used a new mixed-coded GA by using different crossover and mutation operators for each type of variable. For different freshwater demands, the total annual cost that satisfies desired electricity and freshwater demands was minimized. For water demands lower than 8000 $m^3 \cdot h^{-1}$, the MSF unit with condensing-extraction ST is preferred while the hybrid MSF/RO system with the back pressure ST is preferred for higher demands.

Shakib et al. [11] simulated and optimized a MED system coupled to a GT plant through a one-pressure-level (1P) HRSG by applying two heuristic methods. They solved single and multi-objective optimization problems using GA and particle swarm optimization (PSO). By comparing the performances of both optimization methods, the authors concluded about the preference of PSO over GA.

Compared to deterministic methods, GA methods are not influenced by the guess values, they use the objective function itself rather than derivative information on the objective function and constraints, and they use probabilistic transition rules rather than deterministic rules [14]. However, these GA characteristics do not allow to assure that global optimal solutions are found [14]. GAs converts the original problem into an unconstrained problem with bounded search domain by including a penalty term in the objective function for the equality and inequality constraints. Then, it is extremely difficult for the solution to fulfill the equality constraints, since GA is a stochastic search approach, contrary to

what happens with the use of deterministic approaches. In addition, GAs are in general computationally expensive to solve optimization problems with nonlinear equality and inequality constraints [14] – as happens in problems of thermal engineering – and even more so in optimization problems with many discrete decisions such as the one addressed in this study. Only the usage of global optimization methods can guarantee the globality of the solutions.

Although there are many studies on DPDPs using HRSG considering different assumptions and using different computational tools as mentioned, most of them deal with parametric optimization assuming that the configuration of the system is fixed, obtaining the optimal operating conditions and process-unit dimensions that maximize or minimize a certain objective function (OF). Then, the best system configuration is obtained by comparing the performance of all the examined configurations. The finding of a new configuration by means of this methodology depends heavily on the subjectivity and creativity of the process designer, with the risk that one or more appropriate solutions – e.g. cost-effective configurations – will not be considered. This risk can be reduced if simultaneous optimization approaches are used, as proposed in this work. By applying Mathematical Programming approach, it is possible to embed the candidate configurations in a single model and propose hybridizations between them, with the aim to optimize simultaneously all the trade-offs present in all the configurations, including the hybridized ones. This approach allowed finding novel configurations for MSF desalination systems [15], ARS systems [16], and membrane-based CO_2 capture processes [17]. In this sense, only a few publications applying the simultaneous optimization approach of such DPDPs considering the structure of the HRSG as an optimization variable, together with the process-unit sizes and operating conditions of the entire process, can be found in literature [18-20]; however, a very fewer candidate configurations in HRSG were considered in these studies, consequently involving few opportunities for improvement.

In accordance with Martelli et al. [21], the design optimization problem of complex networks of combined heat and power units, such as DPDPs, including the process configuration as an optimization variable, is still an open challenge. In this sense, this work is motivated by the need and challenge of developing a design tool to optimize simultaneously the synthesis and design of DPDPs considering the integration of GT, HRSG, STs, and MSF system.

In this paper, a MINLP optimization model of a DPDP, derived from a superstructure-based representation of the process, which embeds a large number of candidate structures of HRSG, is used. Series, parallel, and combined series-parallel arrangements of heat exchangers are simultaneously considered. Several revamping case studies for the existing Shuaiba North DPDP, located in Kuwait, are investigated considering different optimization criteria. A revamping case consists in determining the optimal number of heat exchangers in the HRSG, the way that these exchangers should be interconnected, and the optimal operating conditions, in order to maximize the ratio between the freshwater production rate and the total HRSG heat transfer area, while satisfying a fixed, specified electrical power generation level, employing the same GT and MSF system as in the Shuaiba North

plant. A second optimal revamping case for the Shuaiba North plant consisting in the maximization of profit (objective function) is performed, including the possibility to sell extra amounts of electricity and/or freshwater. To this end, a cost model is included into the model used in the previous case. The sale prices of electricity and freshwater are introduced as model parameters, which are varied in the ranges 0–0.5 $\$\cdot kWh^{-1}$ and 0–1.5 $\$\cdot m^{-3}$, respectively.

2 Process description

Dual-purpose power/desalination plants (DPDPs) are an economically attractive option for desalination because the cost is allocated to two products (water and electricity). A MSF desalination plant is powered mainly by low or medium-pressure steam. Figure 1 shows a schematic of a DPDP, which integrates a CCHP plant and a MSF system. The CCHP plant consists of a GT and a HRSG that recoveries heat from the exhaust gases to produce steam for both generating electricity in the STs and producing freshwater in the MSF process. The CCHP and MSF plants are coupled through the main heater (MH).

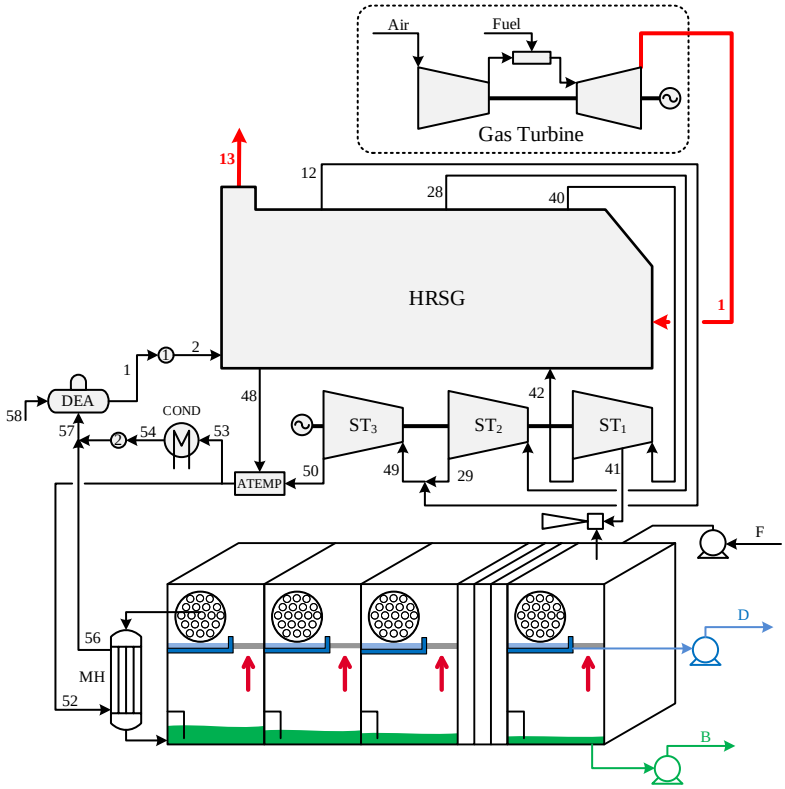

Figure 1. Dual-purpose power/desalination plant.

The optimal design of a DPDP mainly depends on the ratio between the generated power and the produced freshwater. Thus, two extreme design situations are possible: at high ratio values – when the electricity generation level is high but the water demand level is low – and at low ratio values – when the electricity generation level is low but the water demand level is high –; there are many

intermediate situations between these two extremes. The HRSG design can involve 1, 2, or 3 pressure levels with different heat exchanger configurations and include a steam-reheat stage. In turn, the HRSG produces the steam required by STs for electricity generation. In this sense, it should be mentioned that there are different ST types: back-pressure, extraction-condensation, and condensation turbines. The ST types (or the combination of turbines) to use depend on the ratio value.

To optimize the system, all the trade-offs that exist between the total area of the HRSG, heat loads and the corresponding driving forces in the different heat exchangers, the power that must be generated in GT and STs, the operation conditions (flowrate, pressure, and temperature) of the steam that must be produced to power the STs and the MSF system, should be simultaneously elucidated. In addition, the design of DPDP depends on the used optimization criterion; for instance, maximization of the overall system efficiency, minimization of costs, and maximization of profit considering the production of extra amounts of electricity and/or freshwater (if beneficial), as is proposed in a revamping case studied in section 5.2. This is why it is very useful to have a mathematical model that considers all the mentioned trade-offs at the same time and that can systematically determine the optimal design for power-to-freshwater ratio values and optimization criteria established by the user.

3 Mathematical model

The full mathematical model is presented in the Supplementary Material attached to this article. In this section, key aspects about the modeling of the CCPP and MSF systems are only presented. Details about modeling assumptions, numerical values of model parameters are also included in the Supplementary Material.

3.1 Heat recovery steam generator (HRSG)

The model of a HRSG with two pressure levels (2P-HRSG) presented in Manassaldi et al. [22] was properly extended to one with three pressure levels (3P-HRSG), thus increasing the number of candidate structures in the optimization problem. Figure 2 shows a schematic of the proposed superstructure model for the considered DPDP, which integrates the 3P-HRSG model and a MSF system model. The splitter SP1 allows embedding different alternative ways of feeding the working fluid to the 3P-HRSG. All the heat exchangers, including the evaporators, can be selected/removed from the HRSG superstructure model.

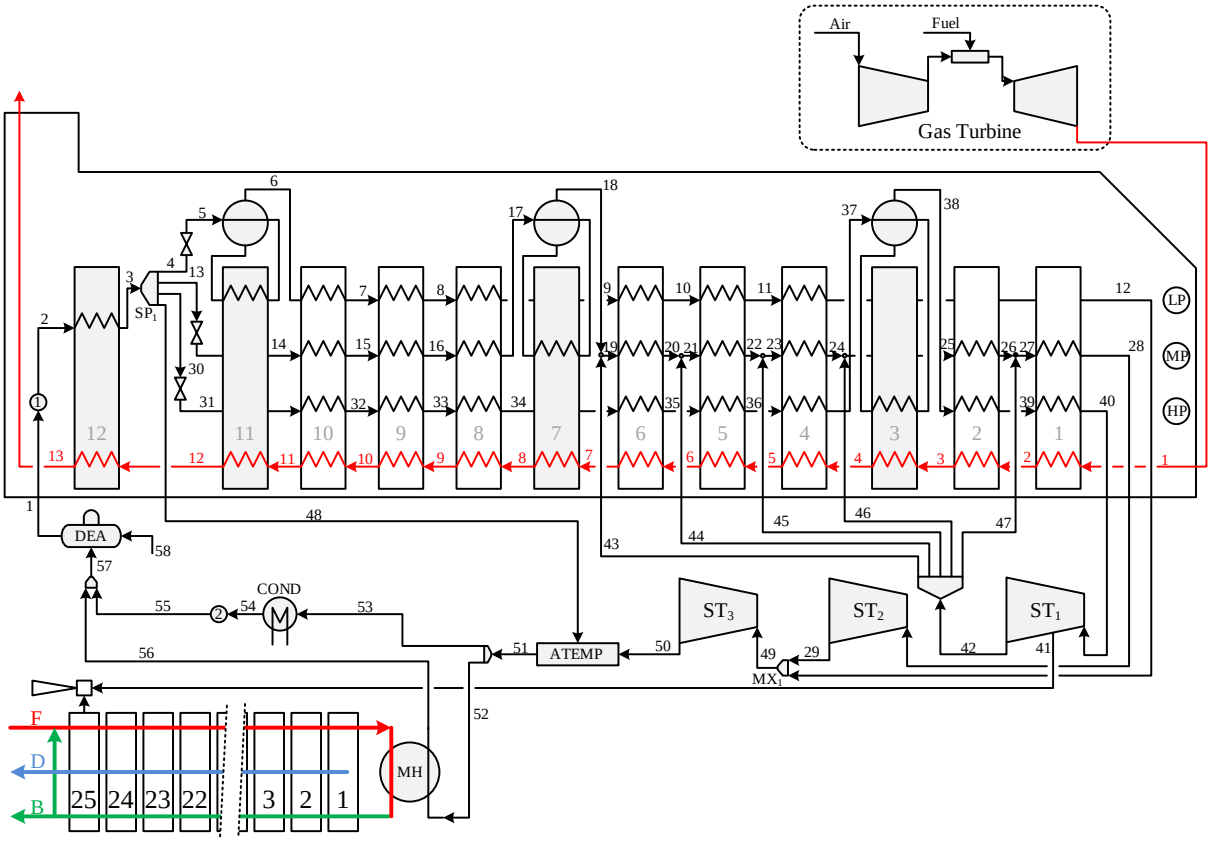

Figure 2. Superstructure representation of the studied DPDP.

As shown in Figure 3a, the HRSG is divided into 12 sections according to the temperature level, with the index i ranging from 1 to 12, and into 4 zones according to the pressure level, with the index j indicating high (HP), medium (MP), and low (LP) pressure levels. The index i=1 refers to the section with the highest temperature of the working fluids. Each heat exchanger of the superstructure can be referred to by the pair (i,j) as is illustrated in Figure 3a. Then, in order to model the selection/removing of a heat exchanger (i,j), a binary variables $x_{i,j}$ is proposed for each exchanger. Thus, for instance, the evaporator working at the LP level is identified by the binary variable $x_{11,LP}$ (Figure 3b). Then, to facilitate the model implementation, a set of elements is defined to relate the heat exchangers with the respective streams of the working fluid of the Rankine cycle (water and saturated and superheated steam) entering/leaving a heat exchanger, and thus, to obtain the set of all exchangers present in the HRSG by linking their section, pressure level, and associated Rankine cycle streams. To this end, the index k is used to refer to a stream of the working fluid of the Rankine cycle that allows to define the set HE(i,j,k).

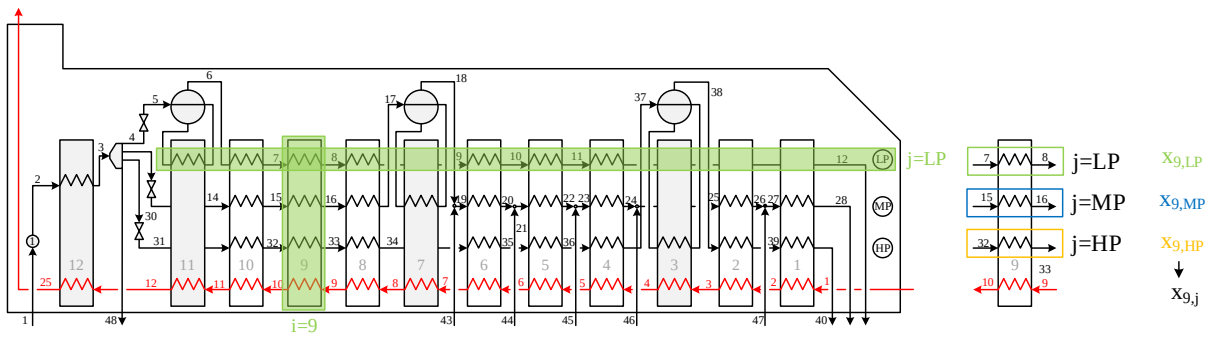

(a)

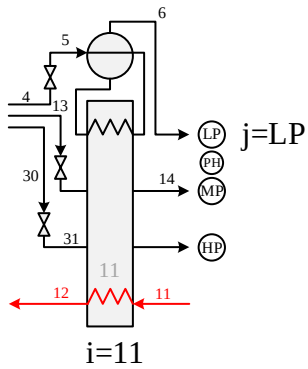

(b)

Figure 3. Location of a heat exchanger in the superstructure representation: (a) candidate heat exchangers in the thermal section i=9; (b) fixed evaporator (11,LP) in the thermal section i=11 at the pressure level j=LP.

Based on the defined indexes, the energy balance in each heat exchanger and its associated heat transfer area are expressed as follows:

$$\sum_{j \in HE(i,j)} \dot{Q}_{i,j} = \dot{m}^G \cdot \left(h_i^G - h_{i+1}^G\right) \qquad \forall i \tag{1}$$

$$\dot{Q}_{i,j} = \dot{m}_k \left(h_{k+1} - h_k\right) \qquad \forall i, j \in HE(i,j,k) \tag{2}$$

$$\dot{Q}_{i,j} = U_{i,j} \cdot A_{i,j} \cdot \Delta T_{i,j} \qquad i, j \in HE(i,j,k) \tag{3}$$

where ΔT is the logarithmic mean temperature difference, which is calculated by the Chen approximation (Eq. (4)):

$$\Delta T_{i,j} = \sqrt[3]{(T_i^G - T_{k+1}) \cdot (T_i^G - T_{k+1}) \cdot \frac{(T_i^G - T_{k+1}) \cdot (T_i^G - T_{k+1})}{2}} \qquad i, j, k \in HE(i,j,k) \tag{4}$$

- Constraints used to select/remove heat exchangers from the superstructure:

To select/remove heat exchangers from the superstructure, constraints (5) and (6) are proposed, which relate the selection of a heat exchanger through the variable $x_{i,j}$ (discrete decision) with its

corresponding heat load $\dot{Q}_{i,j}$ (continuous decision).

$$\sum_{j \in HE(i,j)} \dot{Q}_{i,j} \le x_{i,j} \cdot \left|\dot{Q}_{i,j}\right|_{upper} \qquad i, j \in HE(i, j, k) \tag{5}$$

$$\sum_{j \in HE(i,j)} \dot{Q}_{i,j} \ge x_{i,j} \cdot \left|\dot{Q}_{i,j}\right|_{lower} \qquad i, j \in HE(i, j, k) \tag{6}$$

If $x_{i,j}$=1, then the heat exchanger (i,j) is selected and $\dot{Q}_{i,j} \neq 0$, with $|\dot{Q}_{i,j}|_{lower} \le \dot{Q}_{i,j} \le |\dot{Q}_{i,j}|_{upper}$. Otherwise, if $x_{i,j}$=0, then the heat exchanger is removed and $\dot{Q}_{i,j}$=0.

The model involves the following constraints that are necessary for embedding the candidate configurations, whose mathematical formulations are included in the Supplementary Material (SM).

- Constraints used to avoid equivalent solutions: Eqs. (SM7–SM11).
- Constraints used to select the steam inlet location for reheating: Eqs. (SM12–SM14).
- Constraints for limiting the number of parallel heat exchangers: Eq. (SM15).
- Constraints for allowing repetition of heat exchangers in each pressure level: Eqs. (SM16–SM19).

3.2 Multiple stage flash (MSF) desalination system

Figure 4a and 4b show schematics of the MSF system and a generic flashing stage indicating the optimization variables considered in the model, respectively. The mass and energy balances, design equations used to calculate the dimensions of a flashing chamber (height, length, and width) can be found in the Supplementary Material (Eqs. (SM20–SM41)). The number of stages is a continuous optimization variable. All stages have the same dimensions.

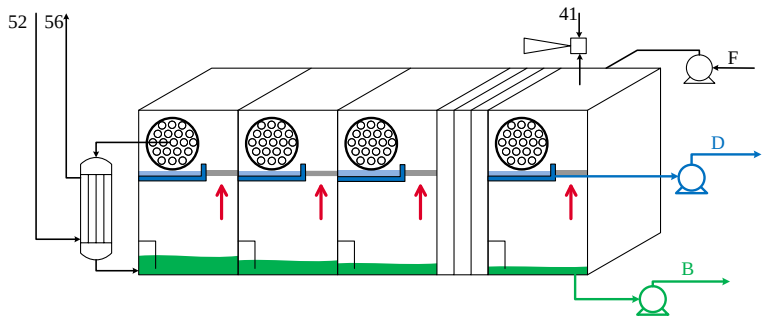

(a)

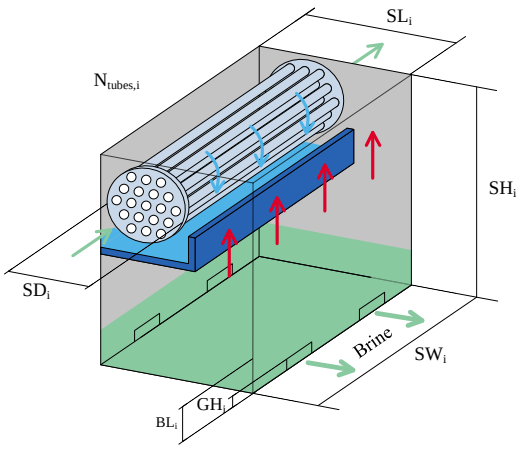

(b)

Figure 4. Schematics of (a) MSF system, (b) generic flashing stage.

3.3 Physicochemical property estimation

Extrinsic functions executed outside the General Algebraic Modeling System optimization software (GAMS) from dynamic-link libraries (DLL) – coded in the programming language C – are used to estimate the thermodynamic properties of both circulating fluids (flue gas and water) at different conditions. The DLL libraries have been developed by the authors and successfully applied in different optimization problems. Details about the implementation of DLLs are available in Manassaldi et al. [23].

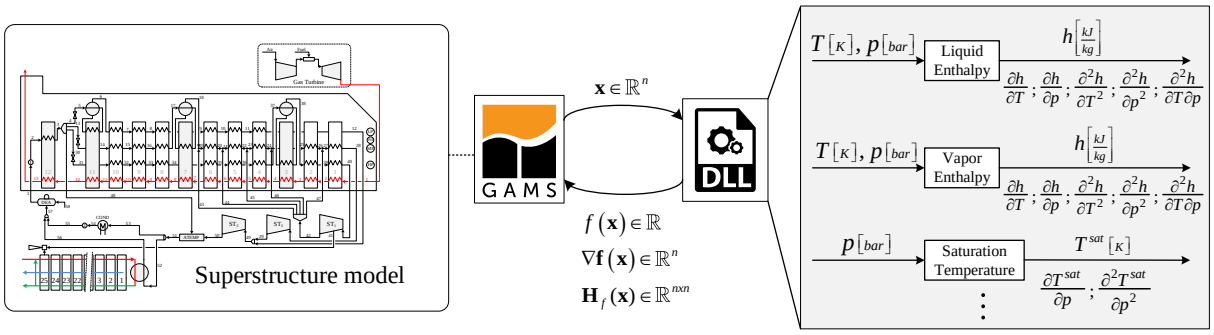

Figure 5. Linking of GAMS to DLL libraries

3.4 Economic model

A complete economic model is considered to calculate the total annual cost (TAC), revenue for selling electricity and freshwater, and profit, which is fully presented in the Supplementary Material (Eqs. (SM46–SM53)). Equations to calculate acquisition costs are those reported in Abu-Zahra et al. [24] and Rao and Rubin [25].

4 Problem statement

Given the superstructure shown in Figure 2, the following two optimization problems for the revamping of the existing Shuaiba North DPDP are proposed:

Optimal revamping problem OR1

$$\text{Max.}\ \frac{\dot{D}}{THTA_{HRSG}}$$

subject to:
-Mass balances
-Energy balances
-Design equations (sizing)
-Physicochemical property estimation equations
-Thermodynamic property estimation equations
-Economic model equations
Process design specifications:
-Fixed net electrical power generation:

$$\dot{W}_{NET.GT} + \dot{W}_{NET,ST} = 288.068\ \text{MW}$$

-Minimum freshwater production: 789.0 $kg \cdot s^{-1}$
Process data
-Seawater temperature: 298 K
-Seawater salinity: 45000 ppm

Optimal revamping problem OR2

$$\text{Max.}\ P_{s,POW}\left(\dot{W}_{NET,GT} + \dot{W}_{NET,ST}\right) + P_{s,WAT}\ \dot{D} - TAC$$

subject to:
-Mass balances
-Energy balances
-Design equations (sizing)
-Physicochemical property estimation equations
-Thermodynamic property estimation equations
- Economic model equations
Process design specifications:
-Minimum net electrical power generation:

$$\dot{W}_{NET.GT} + \dot{W}_{NET,ST} \geq 288.068\ \text{MW}$$

-Minimum freshwater production: 789.0 $kg \cdot s^{-1}$
Process data
-Seawater temperature: 298 K
-Seawater salinity: 45000 ppm

where $\dot{D}$ and $THTA_{HRSG}$ refer to the freshwater (distillate) flowrate and total HRSG heat transfer area, respectively; $P_{s,POW}$ and $P_{s,WAT}$ are model parameters referring to the selling prices for the electrical power and freshwater; TAC is the total annual cost; $\dot{W}_{NET,GT}$ and $\dot{W}_{NET,ST}$ refer to the total net electrical power generated by the gas and steam turbines, respectively.

As a result, the optimal values of the following decision variables are obtained:

- Discrete decisions, which are modelled by using integer variables (0-1):
- Optimal structure (layout) of heat exchangers. This implies to select the number of the heat exchangers and their locations inside the HRSG, indicating how they should be interconnected (in series, series-parallel, or parallel arrangements).

- Optimal number of pressure levels. The results indicate if the HRSG should be operated with three, two, or one pressure levels. For instance, if the HP level is removed, then the associated economizer, evaporator, and superheater must be also removed.
- Optimal location of the reheating stream.
- Continuous decisions:
- Maximal values of the objective functions: $\dot{D} / THTA_{HRSG}$ ratio and profit.
- Optimal values of all cost items and revenue (for selling electricity and freshwater).
- Optimal values of operating conditions (mass flowrate, pressure, temperature, and composition) of all streams and heat loads, and distributions of the total heat transfer areas in HRSG and MSF systems.
- Optimal geometric dimensions of MSF system components (tube length and diameter; flashing chamber height, length, and width).

5 Discussion of results

Firstly, the developed model is verified by comparison of the model outputs with a reference case reported in the literature [26] (existing Shuaiba North DPDP). It consists of 3 GT GE912FA of 215.5 MW each, 3 HRSG, 1 back-pressure ST of 215.7 MW (operated with the steam generated in the three HRSG), and 3 MSF desalination systems of 15 MIGD each. Then, the optimization results obtained by solving the revamping problems formulated in section 4 are discussed in section 5.2.

5.1 Model verification

Figure 6 illustrates the simulated solution obtained considering the input data reported in [26], which is referred to as solution "1P-SimSol". In order to verify the model results, it is necessary to set the same configuration and fix the same values of certain operation variables as in [26], so that the model is solved in simulation mode instead of optimization mode. Verification is performed by comparing the values of the remaining variables. That is, the mathematical model is solved with zero degrees of freedom. Pressure and temperature values of two gas streams are fixed: stream #1a entering HRSG and stream #13 leaving HRSG. Also, the heat load required in the MSF system $(\dot{Q}_{MSF})$ and the freshwater production rate $(\dot{D})$ are fixed during the validation step, whose corresponding values are taken from [26]. The flowrate and temperature of streams #1, #37, and #57 and the electrical power generated in ST are some of the variables used for comparison. It can be concluded that the model outputs are in good agreement with the data reported in [26]. For instance, for stream #1, the flowrate $\dot{D}$ differs only by 0.6 kg·s^{-1} (100.7 vs. 101.3 kg·s^{-1}) and the temperature by 2.5 K (388.9 vs. 386.4 K). Similar differences are observed for streams #37 and #57, while the total net electrical power generated by the steam cycle $\dot{W}_{NET,ST}$ – the difference between the power generated by ST and the

power required by pumps – is slightly higher than that reported in [26] (72.6 vs. 71.7 MW).

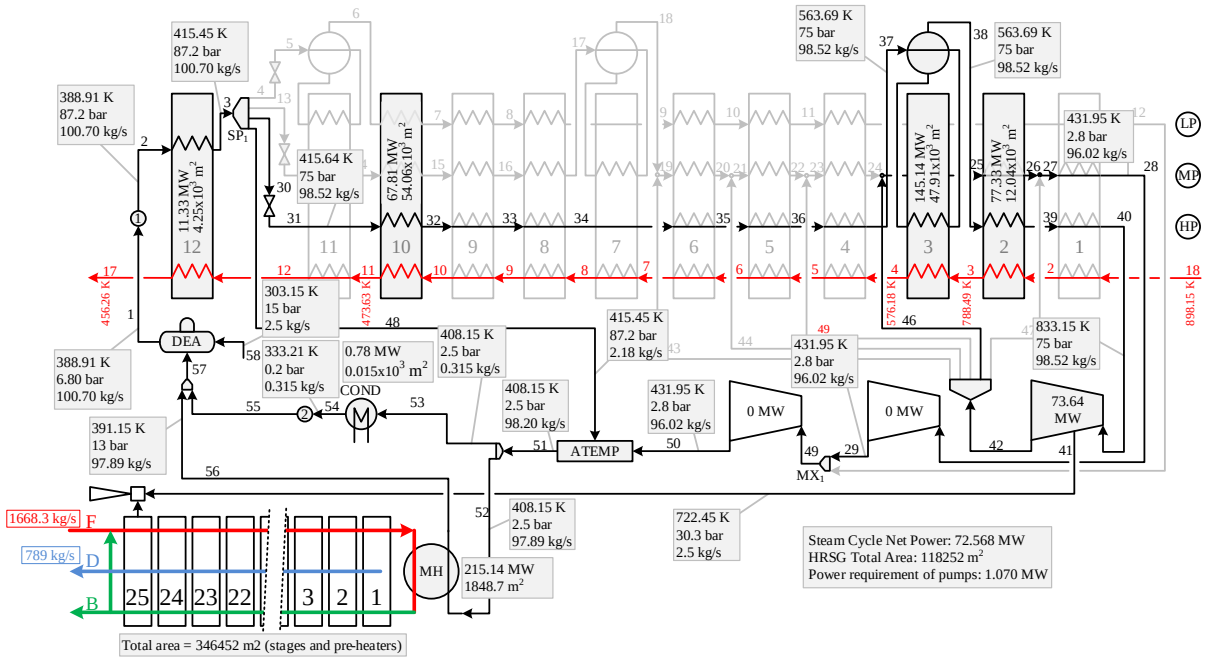

Figure 6. Simulated solution 1P-SimSol obtained for the reference case (Shuaiba North DPDP) [26].

Regarding the MSF system, $\dot{Q}_{MSF}$ and $\dot{D}$ values are fixed at 215.14 MW and 15 MIGD, respectively, as in [26]. The obtained results indicate that the total area required by the MSF system ($THTA_{MSF}$) is 348299.2 m^2, of which 271682.0 m^2 corresponds to the total area of preheaters, 74770.5 m^2 to the area associated with the flashing stage construction, and 1848.7 m^2 to the area of the main heater. The optimal value of the total number of stages reached the upper bound value (25). Figure 7 shows the calculated dimensions of the flashing stages.

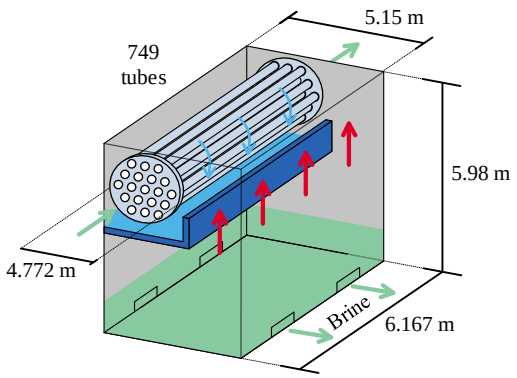

Figure 7. Dimensions of the flashing stages.

5.2 Optimization results

5.2.1 Optimal revamping case OR1

Once verified, the model is used to its maximum potential to solve the optimal revamping problem OR1 proposed in section 4. By maintaining the same characteristics of the gas turbine GT – i.e. operating conditions and total net electrical power generation ($\dot{W}_{NET,GT}$ = 215.500 MW) –, the same total net electrical power generated by the steam turbine ST ($\dot{W}_{NET,ST}$ =72.568 MW), and the same components of the MSF system ($THTA_{MSF}$ = 348299.2 m^2), the aim is to see how much the $\dot{D} / THTA_{HRSG}$ ratio can be increased if the (original) 1P-HRSG is replaced with another one that can operate at 2 or 3 pressure levels with/without steam reheating. To this end, the superstructure-based model presented in the section 3 is solved without imposing any constraints on the structure (configuration) and number of pressure levels of the HRSG.

Figure 8 shows the obtained optimal solution, which is referred to as the solution "3P-OptR1". As can be observed, it selects a HRSG structure consisting of 10 heat exchangers, includes all the 3 pressure levels, and includes steam reheat optimally located. It is worth noting that 2 of the 10 selected heat exchangers operate in parallel. They are the superheater (6,LP), which is located in the section i=6 at the low-pressure level j=LP, and the economizer (6,HP), which is located in the same section at the high-pressure level j=HP. In this section, the gas stream temperature decreases from 595.2 to 533.0 K to transfer 41.416 MW in total (1.626 MW exchanged in the superheater requiring a HTA of 721 m^2, and 39.79 MW exchanged in the economizer requiring a HTA of 19910 m^2). Additionally, the solution 3P-OptR1 proposes first to reheat the steam formed by mixing the steam leaving the turbine ST1 (stream #46) with the steam leaving the first superheater (5,MP), located in the section i=5 at the medium-pressure level j=MP, and then to reheat it in a second superheater (2,MP), located in the section i=2 at the medium-pressure level j=MP, before entering the turbine ST2 (stream #28).

Compared with the simulated solution 1P-SimSol obtained for 1P-HRSG (Figure 6), the optimal solution 3P-OptR1 allows increasing $\dot{D}$ by 14 $kg \cdot s^{-1}$ (803 vs. 789 $kg \cdot s^{-1}$), requiring, in turn, 22753 m^2 less of $THTA_{HRSG}$ (95499 vs. 118252 m^2). Regarding electrical power generation, it can be seen in Figure 8 that that ST3 is the turbine with the highest contribution to $\dot{W}_{NET,ST}$ followed by ST1 (ST3, ST1, and ST2 contributes with 35.48, 23.26, and 14.82 MW, respectively).

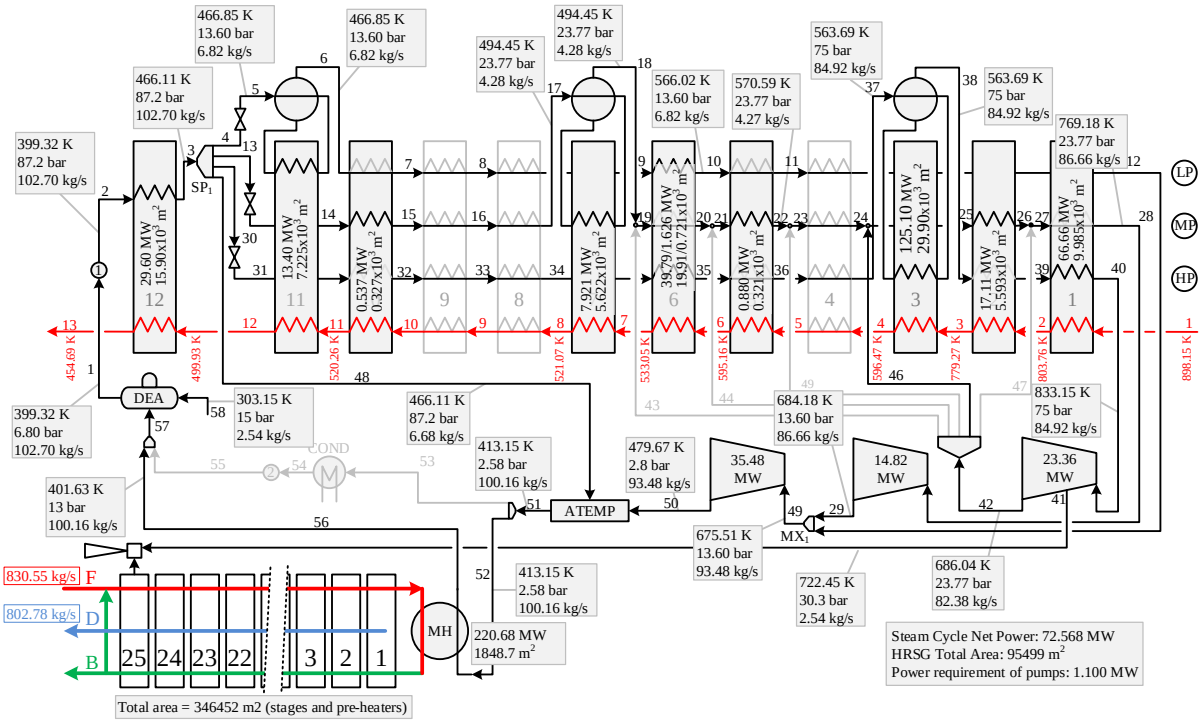

Figure 8. Optimal solution 3P-OptR1 obtained by the MINLP model.

Considering the same GT (i.e. flowrate and temperature of the flue gas entering the HRSG) and the same MSF system (i.e. the same heat transfer areas required by the main heater and preheaters and dimensions of the flashing chambers) as in the 3P-OptR1 solution, the same optimization model is solved but now restricting the number of pressure levels in the HRSG to 2. The solution obtained for this case is shown in Figure 9, which is referred to as solution 2P-OptR1 The fact of allowing only 2 pressure levels reduces the degrees of freedom of the previous optimization problem (with 3 pressure levels), so the solution obtained for this case is a sub-optimal solution with respect to 3P-OptR1. Then, with this new optimization problem, it is proposed to investigate how much better a HRSG operating with 2 pressure levels performs with respect to a HRSG operating with 1 pressure level (1P-SimSol) and how much worse it performs with respect to one operating with 3 pressure levels (optimal solution 3P-OptR1). Table 1 compares the objective function and main process variable values obtained in 1P-SimSol, 2P-OptR1, and 3P-OptR1.

According to Figure 9, the optimal structure obtained in 2P-OptR1 involves 6 heat exchangers i.e. 3 less than in 3P-OptR1 due to the elimination of a pressure level from the problem formulation, and consequently, the economizer, evaporator, and superheater associated to it.

According to Table 1, if the 3P-HRSG is replaced with a 2P-HRSG while maintaining unchanged the variables related to the GT and MSF systems, $\dot{D}$ increases by 10.675 kg·s^{-1} (813.457 vs. 802.782 kg·s^{-1}). However, $THTA_{HRSG}$ increases by 9956 m^2 (105455 vs. 95499 m^2), thus resulting in a lower value of the objective function – $\dot{D}/THTA_{HRSG}$ ratio – decreasing from 8.406×10^{-3} to 7.714×10^{-3} kg·s^{-1}·m^{-2}. The total HTA required in economizers and evaporators increase by 10687 m^2

and 3625 m^2, respectively, with respect to those in 3P-OptOR1 (46817 vs. 36130 m^2 and 46374 vs. 42749 m^2) while the total HTA required in superheaters is reduced by 4355 m^2 (12264 vs. 16619 m^2).

If the 1P-HRSG (Shuaiba North) GTCC plant is replaced with a 2P-HRSG while maintaining the same GT and MSF systems, the $\dot{D}$ / THTA$_{HRSG}$ ratio increases from 6.672 to 7.714 kg·s^{-1}·m^{-2} due to the increase in $\dot{D}$ by 24.457 kg·s^{-1} (813.457 vs. 789.0 kg·s^{-1}) and the decrease in THTA$_{HRSG}$ by 12797 m^2 (105455 vs. 118252 m^2). The total HTA required in economizers and evaporators decrease by 11493 m^2 and 1537 m^2, respectively, with respect to 1P-SimSol (46817 vs. 58310 m^2 and 46374 vs. 47911 m^2) while the total HTA required by superheaters increases by 233 m^2 (12264 vs. 12031 m^2).

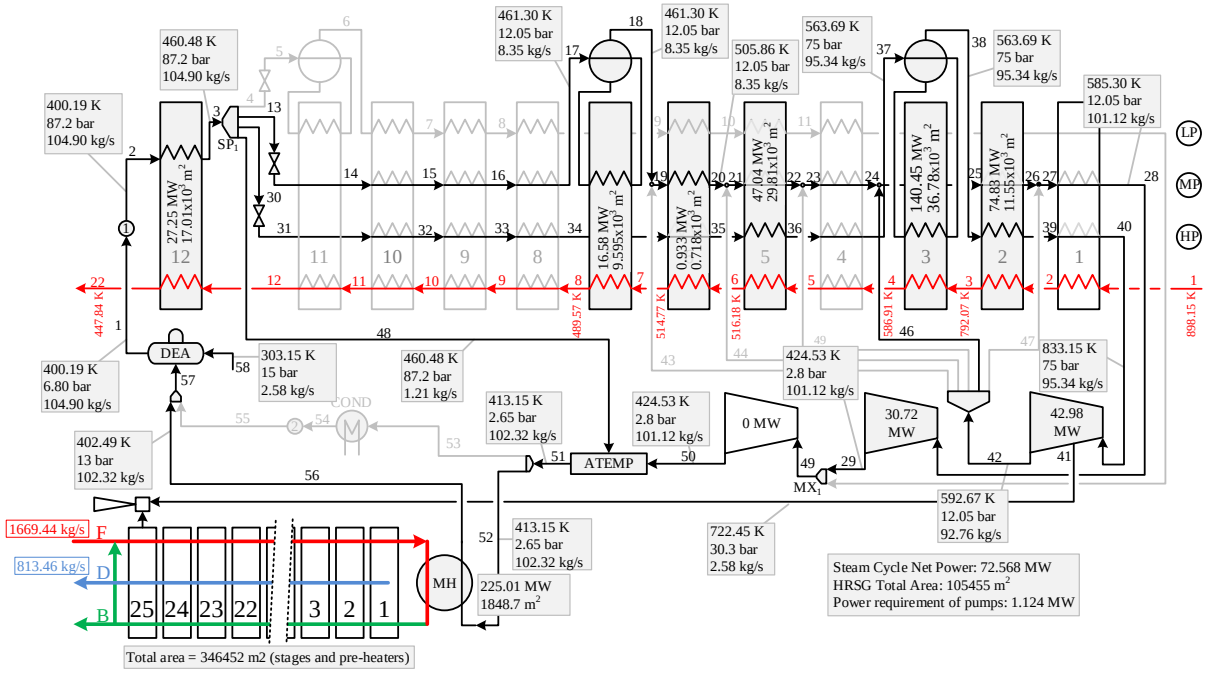

Figure 9. Optimal solution 2P-OptR1 obtained by limiting the number of pressure levels to 2.

Regarding the behavior of the steam turbines, it can be seen in Figure 9 that the power generation rates of ST1 and ST2 increase by around twice to meet the specified $\dot{W}_{NET,ST}$ (72.568 MW) with respect to 3P-OptR1 (42.98 vs. 23.36 MW in ST1 and 30.72 vs. 14.82 MW in ST2).

Table 1. Comparison of the 1P-SimSol, 2P-OptR1, and 3P-OptR1 solutions ($\dot{W}_{NET,GT}$ =215.5 MW)

	1P-SimSol	2P-OptR1	3P-OptR1
Obj. function, $\dot{D}$ / THTA$_{HRSG}$ ratio (kg·s^{-1}·m^{-2})	6.672×10^{-3}	7.714×10^{-3}	8.406×10^{-3}
Freshwater production rate, $\dot{D}$ (kg·s^{-1})	789.0	813.457	802.782
Total area in HRSG, THTA$_{HRSG}$ (m^2)	118252	105455	95499
– Economizers	58310	46817	36130
– Evaporators	47911	46374	42749
– Superheaters	12031	12264	16619
Total heat load in HRSG, $\dot{Q}_{HRSG}$ (MW)	301.609	307.081	302.627
Total flowrate of working fluid, $\dot{m}_f$ (kg·s^{-1})	100.70	104.901	102.701

Total net electric power by STs, $\dot{W}_{NET,ST}$ (MW)	72.568 #	72.568 #	72.568 #
– HP ST (ST1)	73.638	42.976	23.362
– MP ST (ST2)	–	30.716	14.819
– LP ST (ST3)	–	–	35.487

Fixed value.

5.2.2 Optimal revamping case OR2

This section presents the results obtained when solving the optimal revamping problem OR2, which differs from the problem OR1 in that $\dot{W}_{NET,ST}$ is now a free variable – unlike in OR1, where it was a (fixed) model parameter – and the objective function is to maximize the profit – the difference between the revenue for selling electricity and freshwater and the total cost –. Regarding the system components, it is considered that the characteristics (sizes) of the GT and MSF systems are the same as in the previous case (Shuaiba North DPDP), while the configuration (structure), sizes, and operation conditions of the HRSG, and the operation conditions of the MSF system are considered as optimization variables. The sale prices of electricity ($P_{s,POW}$) and freshwater ($P_{s,WAT}$) are parametrically varied between 0 and 0.5 $\$\cdot kWh^{-1}$ and between 0 and 1.5 $\$\cdot m^{-3}$, respectively. It is emphasized that the objective is not to determine the sale prices of electricity and freshwater but to investigate how the optimal design of the HRSG and the optimal operating conditions of the MSF system vary with different pairs ($P_{s,POW}$, $P_{s,WAT}$), and to determine the corresponding optimal $\dot{W}_{NET,ST}$ and $\dot{D}$ values. The production rates required in OR1 ($\dot{W}_{NET,ST}$ =72.568 MW and $\dot{D}$ =789.0 $kg\cdot s^{-1}$) are set as lower bound values in this optimization problem.

Table 2 shows the maximum objective function (profit) values and optimal values of $\dot{W}_{NET,ST}$, $\dot{D}$, TAC, $\dot{Q}_{MSF}$, and $THTA_{HRSG}$ for each pair ($P_{s,POW}$, $P_{s,WAT}$). A first conclusion to highlight from the process configuration point of view is that, for all cases, the optimal system configuration is the same as in the previous case; that is, the model selects 3 pressure levels in the HRSG with a total of 10 heat exchangers (3 economizers, 3 evaporators, and 4 superheaters). In addition, stream #46 is also selected for reheat. As illustration, Figure 10 presents the optimal solution obtained for $P_{s,POW}$=0.25 $\$\cdot kWh^{-1}$ and $P_{s,WAT}$ =0.7 $\$\cdot m^{-3}$, implying an optimal $\dot{W}_{NET,ST}$ of 76.908 MW and optimal $\dot{D}$ of 828.29 $kg\cdot s^{-1}$.

Table 2 indicates that for $P_{s,POW}$=0 and $P_{s,WAT}$=0, profit maximization is equivalent to TAC minimization; therefore, $\dot{W}_{NET,ST}$ and $\dot{D}$ reached the lower bounds on these variables (72.568 MW and 789.0 $kg\cdot s^{-1}$), as expected. For $P_{s,POW}$=0 and $P_{s,WAT}\neq 0$, $\dot{D}$ increases with increasing $P_{s,WAT}$ values until $P_{s,WAT}$=1.4 $\$\cdot m^{-3}$, for which $\dot{D}$ reaches its highest value, thus indicating that a greater $\dot{D}$ value is not economically convenient since the investment cost required by the HRSG would grow faster than the associated revenue; therefore, the profit would be negatively affected. If $P_{s,WAT}$ is increased from 1.4 to 1.5 $\$\cdot m^{-3}$, the profit increases 2.408×10^{-6} $\$\cdot yr.^{-1}$ and is only due to the increase in $P_{s,WAT}$ since

$\dot{D}$, TAC, and $THTA_{HRSG}$ remain constant in 835.857 kg·s^{-1}, 141.427×10^{-6} \$·yr.$^{-1}$, and 108612 m^2, respectively. For $P_{s,POW}$=0 and $P_{s,WAT}$ ranging between 0 and 1.5 \$·m^{-3}, it is observed that the sign of the objective function (profit) is negative, indicating that TAC dominates the revenue for selling water. For $P_{s,POW}$=0.05 \$·kWh^{-1}, it is not convenient to generate more $\dot{W}_{NET,ST}$ than the required level (72.568 MW) due to the increased investment requirement – as a consequence of larger steam turbines and/or $THTA_{HRSG}$ – is greater than the obtained revenue. Similarly to the previous case, when $P_{s,WAT}$ is increased, $\dot{D}$ increases until reaching the maximum value of 835.857 kg·s^{-1}, what happens for $P_{s,WAT}$=1.4 \$·m^{-3}. It can also be observed that the increase in $P_{s,WAT}$ from 1.0 to 1.1 \$·m^{-3} inverts the sign of the profit from negative to positive, thus indicating that the revenue for selling both products begins to be greater than the associated total cost. Table 2 also indicates that, regardless $P_{s,WAT}$, it is always economically convenient to generate extra electricity if $P_{s,POW}$ is equal or higher than 0.1 \$·kWh^{-1} since the revenue for selling electricity exceeds the increase in the required investment cost. For instance, compared to the pair (0.05 \$·kWh^{-1}, 0 \$·m^{-3}), when $P_{s,POW}$=0.1 \$·kWh^{-1}and $P_{s,WAT}$=0 \$·m^{-3}, an additional amount of 0.469 MW of power is generated, resulting in an increase in the profit by 115.238×10^{-6} \$·yr.$^{-1}$, at the cost of increasing the $THTA_{HRSG}$ by 4484 m^2. Compared to $P_{s,POW}$=0.1 \$·kWh^{-1} and $P_{s,WAT}$=0 \$·m^{-3}, an additional amount of 13.318 kg·s^{-1} of water and 90.50 kW of power are produced when $P_{s,WAT}$=0.1 \$·m^{-3}, resulting in an increase in profit by 2.295×10^{-6} \$·yr.$^{-1}$.

Table 2. Main 3P-OptR2 optimal values obtained for different selling prices ($\dot{W}_{NET,GT}$ =215.5 MW).

$P_{s,POW}$ (\$/kWh)	$P_{s,WAT}$ (\$/m^3)	Profit (×10^{-6} \$/yr.)	TAC (×10^{-6} \$/yr.)	$\dot{W}_{NET,ST}$ (MW)	$\dot{D}$ (kg/s)	$THTA_{HRSG}$ (m^2)	$\dot{Q}_{MSF}$ (MW)
0.0	0.0	−140.634	140.634	72.568	789.000	94988	218.325
	0.1	−138.345	140.645	72.568	798.577	95161	218.981
	0.2	−136.042	140.657	72.568	801.210	95334	220.041
	…	…	…	…	…	…	…
	1.3	−110.129	141.343	72.568	833.699	107119	233.333
	1.4	−107.725	141.427	72.568	835.857	108612	234.223
	1.5	−105.317	141.427	72.568	835.857	108612	234.229
0.05	0.0	−25.407	140.634	72.568	789.000	94988	218.325
	0.2	−20.815	140.657	72.568	801.210	95334	220.041
	…	…	…	…	…	…	…
	1.0	−2.073	141.090	72.568	826.046	102681	230.169
	1.1	0.310	141.172	72.568	828.764	104115	231.290
	1.2	2.700	141.257	72.568	831.317	105601	232.346
	…	…	…	…	...	…	…
	1.4	7.502	141.427	72.568	835.857	108612	234.229
	1.5	9.718	141.618	72.568	835.857	112103	234.229
0.1	0	89.831	140.998	73.037	789.000	99473	219.719
	0.1	92.126	141.087	73.127	802.317	100655	220.488
	0.2	94.441	141.221	73.279	805.414	102414	221.740
	…						
	0.9	110.865	141.895	73.777	823.252	112420	229.018
	1	113.239	141.954	73.783	825.235	113468	229.834
	1.1	115.618	142.007	73.775	827.165	114445	230.630
	1.2	118.003	142.052	73.754	829.052	115350	231.409
	1.3	120.394	142.090	73.718	830.907	116186	232.176

	1.4	122.789	142.121	73.667	832.741	116952	232.936
	1.5	125.190	142.144	73.602	834.565	117648	233.692
0.15	0.0	205.773	143.200	75.311	789.000	130808	226.136
	0.1	208.075	143.218	75.286	816.204	131277	226.129
	0.2	210.428	143.293	75.343	817.482	132475	226.652
	…	…	…	…		…	…
	1.3	236.531	143.898	75.640	829.615	143107	231.642
	1.4	238.921	143.935	75.643	830.461	143821	231.991
	1.5	241.314	143.969	75.642	831.290	144503	232.335
0.25	0.0	439.183	145.598	76.890	789.000	173101	230.283
	0.1	441.455	145.598	76.890	789.000	173101	230.283
	0.2	443.820	145.615	76.839	826.032	173732	230.163
	…	…	…	…	…	…	…
	0.7	455.732	145.782	76.907	828.291	177022	231.095
	0.8	458.118	145.799	76.912	828.663	177371	231.248
	0.9	460.505	145.792	76.906	828.923	177258	231.356
	…						
	1.5	474.843	145.737	76.851	830.521	176282	232.016
0.5	0.0	1024.422	146.135	77.139	789.000	183742	230.719
	0.1	1026.694	146.135	77.139	789.000	183742	230.719
	0.2	1028.967	146.135	77.139	789.000	183742	230.719
	0.3	1031.305	146.120	77.070	826.714	183739	230.444
	0.4	1033.686	146.119	77.070	826.803	183722	230.480
	0.5	1036.068	146.118	77.070	826.891	183705	230.517
	…	…	…	…	…	…	…
	1.4	1057.511	146.107	77.061	827.698	183505	230.850
	1.5	1059.895	146.106	77.060	827.789	183479	230.887

For $P_{s,POW}$=0.1 $\$\cdot kWh^{-1}$ and increasing $P_{s,WAT}$ values, $\dot{W}_{NET,ST}$ increases until $P_{s,WAT}$=1.0 $\$\cdot m^{-3}$, reaching the value of 73.783 MW, which implies of $\dot{D}$ value of 825.235 $kg\cdot s^{-1}$. However, for increasing $P_{s,WAT}$ values greater than 1.0 $\$\cdot m^{-3}$, $\dot{W}_{NET,ST}$ decreases slightly since the revenue for selling water is higher than the revenue that can be obtained by generating more electricity.

On the other hand, it is also important to note that, for any fixed $P_{s,WAT}$ value, for instance 1.5 $\$\cdot m^{-3}$, the electricity generation for $P_{s,POW}$ = 0.10 $\$\cdot kWh^{-1}$ increases by 1.034 MW with respect to $P_{s,POW}$=0.05 $\$\cdot kWh^{-1}$, and prevents water production from reaching the maximum $\dot{D}$ value for 0.05 $\$\cdot kWh^{-1}$ (835.857 $kg\cdot s^{-1}$). In other words, the generation of extra electricity tends to decrease the maximum attainable production of extra freshwater. This behavior maintains with increased $P_{s,POW}$ values, as shown in Table 2. For instance, the electricity generation for $P_{s,POW}$ = 0.5 $\$\cdot kWh^{-1}$ increases by 0.210 MW with respect to $P_{s,POW}$=0.25 $\$\cdot kWh^{-1}$, at the cost of decreasing the water production rate from 830.521 $kg\cdot s^{-1}$ to 827.789 $kg\cdot s^{-1}$.

The comparison of Figures 8 and 10 allow to observe how the flowrates, pressures, and temperatures of the circulating fluid within the HRSG differ between 3P-OptR1 (max. of $\dot{D}$ / $THTA_{HRSG}$ ratio) and 3P-OptR2 (max. of profit for $P_{s,POW}$=0.25 $\$\cdot kWh^{-1}$ and $P_{s,WAT}$=0.7 $\$\cdot m^{-3}$).

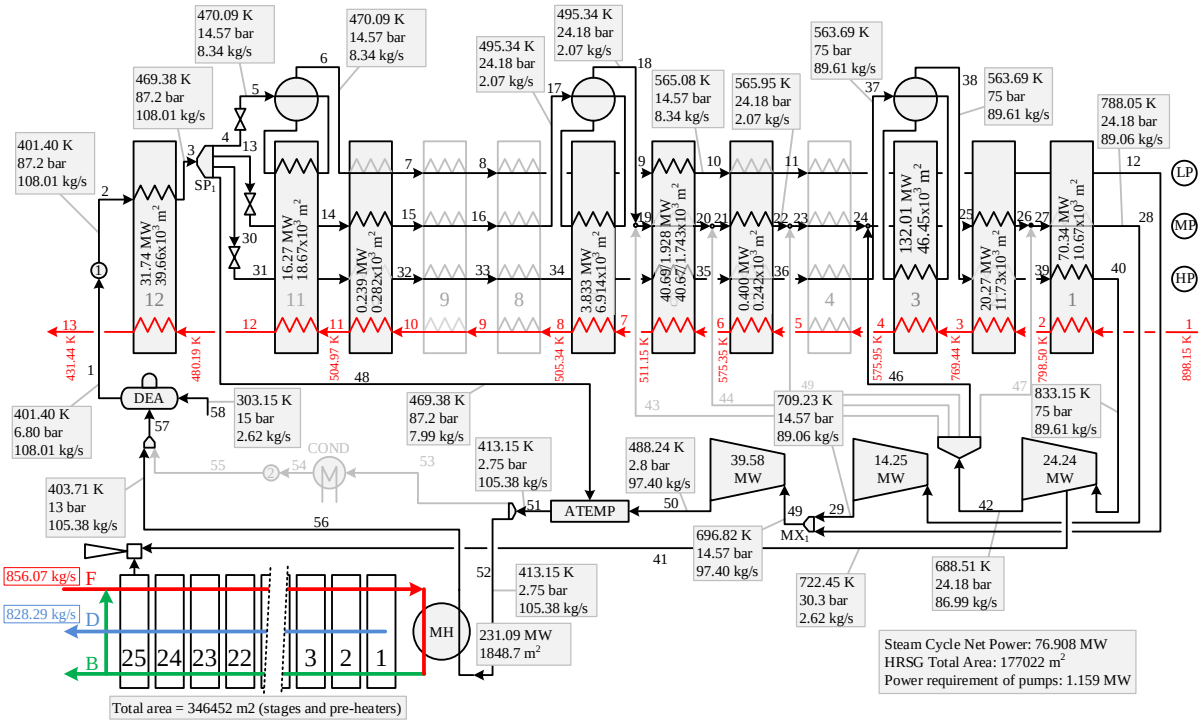

Figure 10. Optimal solution 3P-OptR2 ($P_{s,POW}$=0.25 \$·kWh^{-1} and $P_{s,WAT}$=0.7 \$·m^{-3}).

Regarding electricity generation, the comparison of Figures 8 and 10 shows that the 3P-OptR2 solution produces 76.908 MW, that is, 4.340 MW more power than 3P-OptR1, and that ST3 and ST2 generate the largest and smallest amounts, respectively, in both solutions. The power increase in 3P-OptR2 is due to the increase in the circulating fluid flowrate in HRSG and the steam conditions at the turbines inlet, mainly in ST3, which is the largest contributor. According to Figure 10, the pressure and temperature of stream #49 leaving the mixer MIX1, which mixes stream #12 (LP steam) and stream #29 (steam leaving ST2), play an important role to reach the ST3 inlet conditions and, thus, increase its generation level. In 3P-OptR2, the mixer MIX1 operates at 0.97 bar higher than in 3P-OptR1 (14.57 vs. 13.60 bar), which allows increasing the temperature of stream #49 by 21.3 K with respect to that in 3P-OptR1 (696.8 vs. 675.5 K), thus increasing the steam quality at the ST3 inlet. Since the ST3 flowrate in 3P-OptR2 is 5.310 kg·s^{-1} higher than in 3P-OptR1 and the steam expands to the same pressure in ST3 (2.8 bar) in both solutions, the power generated in 3P-OptR2 is 4.100 MW higher. The operating mode of ST3 in 3P-OptR2 implies small variations in the input and output conditions of ST1 and ST2, but generating practically the same power levels as in 3P-OptR1. It is important to mention that changes in the turbine operating conditions (mainly pressure) cause – through the resulting driving forces – increases in the heat transfer areas of the HRSG components and, consequently, in their associated investment requirements. However, the increased investment is lesser than the revenue for selling the extra amount of electricity generated, thus resulting in a higher profit.

Regarding the freshwater production, it is observed that, for the considered sale prices, the maximum profit is obtained with an optimal $\dot{D}$ of 828.290 kg·s^{-1}, i.e. by producing 25.510 kg·s^{-1} more than 3P-OptR1. To achieve this production, the MSF main heater requires increasing the heat load by 10.41 MW with respect to 3P-OptR1 (231.09 vs. 220.68 MW), which is satisfied by increasing the steam requirement in the MSF main heater by 5.220 kg·s^{-1} (105.380 vs. 100.160 kg·s^{-1}).

5.2.3 Sub-optimal revamping case. Profit maximization of the 1P-HRSG configuration.

The same optimization problem (profit maximization) was solved for the configuration of the existing Shuaiba North GTCC DPDP (1P-SimSol). To this end, the binary variables were appropriately set to 0/1 in order to fix this configuration in the superstructure model. Therefore, this optimization problem involves far fewer degrees of freedom with respect to the previous ones because many candidate configurations embedded in the model are no longer considered. It is then expected that the optimal solutions are worse with respect to the previous ones. The profit was maximized by parametrically varying $P_{s,POW}$ between 0 and 0.5 \$·kWh^{-1} and $P_{s,WAT}$ between 0 and 1.5 \$·m^{-3}. All obtained results are reported in the Supplementary Material. Table 3 lists some selected results for discussion. The new set of "sub-optimal" solutions is useful as it allows having a new sub-optimized revamping case for comparison purposes.

Similarly to the previous case (Table 2 and Figure 10), an illustrative optimal solution corresponding to the same sale prices of electricity ($P_{s,POW}$=0.25 \$·kWh^{-1}) and freshwater ($P_{s,WAT}$=0.7 \$·m^{-3}) is presented in Table 3 and Figure 11. By comparing the solutions in Tables 2 and 3, similar behaviors of profit, TAC, $\dot{W}_{NET,ST}$, and $\dot{D}$ values are observed between 3P-OptR2 and 1P-OptR2 but showing different numerical values. For instance, the convenience of generating extra electricity begins at $P_{s,POW}$=0.15 \$·kWh^{-1} instead of 0.10 \$·kWh^{-1}, as happens in 3P-OptR2. While the convenience of producing extra freshwater begins at $P_{s,WAT}$=0.1 \$·m^{-3}, similar as in 3P-OptR2. The amounts of electricity and freshwater obtained in 1P-OptR2 are lower than in 3P-OptR2 and, consequently, the corresponding profits. Because the GT capacity is kept fixed at the same value, extra productions of both electricity and freshwater in 1P-OptR2 are strongly limited because there are not enough degrees of freedom to conveniently modify the operation conditions in the HRSG to achieve improved profit values.

Table 3. Main 1P-OptR2 optimal values obtained for different selling prices ($\dot{W}_{NET,GT}$ =215.5 MW).

$P_{s,POW}$ (\$/kWh)	$P_{s,WAT}$ (\$/m^3)	Profit (×10^{-6} \$/yr.)	TAC (×10^{-6} \$/yr.)	$\dot{W}_{NET,ST}$ (MW)	$\dot{D}$ (kg/s)	$THTA_{HRSG}$ (m^2)	$\dot{Q}_{MSF}$ (MW)
0.0	0.0	−141.831	141.831	72.568	789.000	116473	215.709
	0.1	−139.557	141.834	72.568	790.407	116521	215.704
	…	…	…	…	…	…	…
	1.4	−109.964	141.834	72.568	790.407	116521	215.704
	1.5	−107.688	141.834	72.568	790.407	116521	215.704
0.05	0.0	−26.604	141.831	72.568	789.000	116473	215.709

	0.1	−24.330	141.834	72.568	790.407	116521	215.704
	…	…	…	…	…	…	…
	1.1	−1.567	141.834	72.568	790.407	116521	215.704
	1.2	0.710	141.834	72.568	790.407	116521	215.704
	…	…	…	…	…	…	…
	1.5	7.539	141.834	72.568	790.407	116521	215.704
0.1	0.0	88.623	141.831	72.568	789.000	116473	215.709
	0.1	90.897	141.834	72.568	790.407	116521	215.704
	0.2	93.173	141.834	72.568	790.407	116521	215.704
	…	…	…	…	…	…	…
	1.5	122.766	141.834	72.568	790.407	116521	215.704
0.15	0.0	203.850	141.831	72.568	789.000	116473	215.709
	0.1	206.124	141.834	72.568	790.407	116521	215.704
	….	…	…	…	...	…	…
	1.4	235.768	142.440	73.013	793.466	126106	216.928
	1.5	238.054	142.489	73.046	793.694	126911	217.020
0.25	0.0	434.650	142.588	73.119	789.000	128508	217.236
	0.1	436.922	142.588	73.119	789.000	128508	217.236
	0.2	439.208	142.586	73.110	794.133	128509	217.195
	…	…	…	…	…	…	…
	1.5	468.940	142.586	73.110	794.133	128509	217.195
0.5	0.0	1011.888	142.588	73.119	789.000	128508	217.236
	0.1	1014.160	142.588	73.119	789.000	128508	217.236
	0.2	1016.432	142.588	73.119	789.000	128508	217.236
	0.3	1018.715	142.586	73.110	794.133	128509	217.195
	0.4	1021.002	142.586	73.110	794.133	128509	217.195
	…	…	…	…	…	…	…
	1.5	1046.160	142.586	73.110	794.133	128509	217.195

Table 4. Comparison of values between 1P-OptR2 and 3P-OptR2 solutions ($\dot{W}_{NET,GT}$ =215.5 MW).

	$P_{s,POW}$ (\$/kWh)	$P_{s,WAT}$ (\$/m^3)	Profit ($\times10^{-6}$ \$/yr.)	TAC ($\times10^{-6}$ \$/yr.)	$\dot{W}_{NET,ST}$ (MW)	$\dot{D}$ (kg/s)	$THTA_{HRSG}$ (m^2)	$\dot{Q}_{MSF}$ (MW)
1P	0.0	0.0	−141.831	**141.831****	72.568	789.000	116473	215.709
3P			−140.634	140.634	72.568	789.000	94988	218.325
1P	0.5	1.5	**1046.160***	142.586	73.110	794.133	128509	217.195
3P			1059.895	146.106	77.060	827.789	183479	230.887
1P	0.25	0.0	434.650	142.588	**73.119**#	789.000	128508	217.236
3P			439.183	145.598	76.890	789.000	173101	230.283
1P	0.25	0.2	439.208	142.586	73.110	**794.133**#	128509	217.195
3P			443.820	145.615	76.839	826.033	173732	230.163

* Maximum value by maximizing profit
** Minumun value by maximizing profit
# Highest value obtained by maximizing profit.

Table 4 compares the main process variables based on 1P-OptR2. First, the solution values obtained for $P_{s,POW}$=0 and $Ps,_{WAT}$=0 are reported, for which maximizing profit is equivalent to minimizing TAC, as is observed. In this case, no extra amounts of electricity and freshwater are produced with respect to the desired minimum requirements (72.568 MW and 789.0 kg·s^{-1}, respectively). The minimum TAC value obtained in 1P-OptR2 is 1.197×10^{-6} \$·yr.$^{-1}$ higher than in 3P-OptOR2 due to the increase in $THTA_{HRSG}$ by 21485 m^2 (from 94988 to 116473 m^2). Second, the solution values obtained for $P_{s,POW}$=0.5 \$·kWh^{-1} and $P_{s,WAT}$=1.5 \$·m^{-3} are reported. This pair of sale prices lead to the maximum attainable profit computed by 1P-OptR2, which is compared with the

maximum profit obtained by 3P-OptR2 for this pair of sale prices. Third, the solution values obtained for $P_{s,POW}$=0.25 $\$\cdot kWh^{-1}$ and $Ps,_{WAT}$=0 are reported. This pair of sale prices leads to the highest value of $\dot{W}_{NET,ST}$ obtained by 1P-OptR2 (73.119 MW) when the profit is maximized, and it is compared with the obtained by 3P-OptR2 (76.890 MW) for the same sale prices. These $\dot{W}_{NET,ST}$ values are respectively 0.551 MW and 4.322 MW higher than the minimum desired power generation (72.658 MW). Forth, the solution values obtained for $P_{s,POW}$=0.25 $\$\cdot kWh^{-1}$ and $Ps,_{WAT}$=0.2 $\$\cdot m^{-3}$ are reported. This pair of sale prices leads to the highest value of $\dot{D}$ obtained by 1P-OptR2 (794.133 $kg\cdot s^{-1}$), and it is compared with the obtained by 3P-OptR2 (826.033 $kg\cdot s^{-1}$) for the same sale prices. These $\dot{D}$ values are respectively 5.133 $kg\cdot s^{-1}$ and 37.033 $kg\cdot s^{-1}$ higher than the minimum desired freshwater production (789.0 $kg\cdot s^{-1}$), which is imposed as a lower bound. It is important to emphasize that the values of $\dot{D}$ and $\dot{W}_{NET,ST}$ in Table 4 were obtained by maximizing profit in all cases (not maximizing $\dot{D}$ or $\dot{W}_{NET,ST}$).

As expected, the maximum profit values obtained in 1P-OptR2 and 3P-OptR2 are achieved at the highest sale prices considered ($P_{s,POW}$=0.5 $\$\cdot kWh^{-1}$ and $P_{s,WAT}$=1.5 $\$\cdot m^{-3}$). The differences in profit values between 1P-OptR2 and 3P-OptR2 increase with the increase of both prices. These differences range between 1.991×10^{-6} $\$\cdot yr.^{-1}$ (computed for $P_{s,POW}$=0.05 $\$\cdot kWh^{-1}$ and $P_{s,WAT}$=1.2 $\$\cdot kWh^{-1}$) and 13.735×10^{-6} $\$\cdot yr.^{-1}$ (computed for 0.5 $\$\cdot kWh^{-1}$ and 1.5 $\$\cdot m^{-3}$).

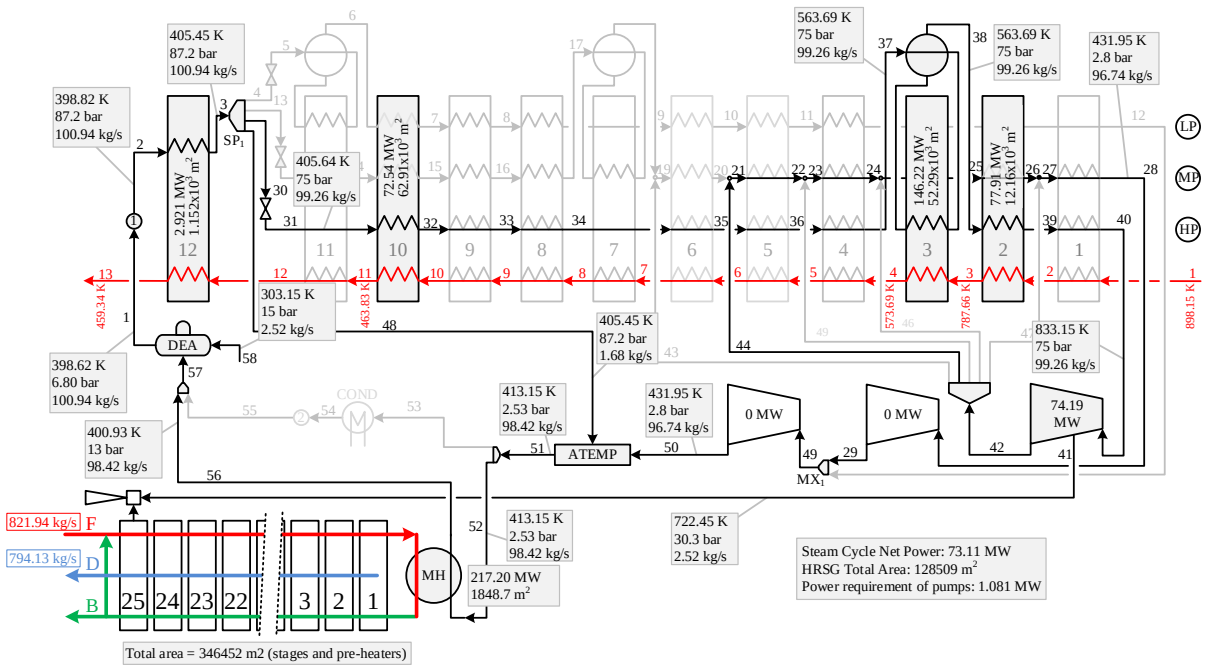

Figure 11. Optimal solution 1P-OptSol obtained by maximizing the profit for $P_{s,POW}$=0.25 $\$\cdot kWh^{-1}$ and $P_{s,WAT}$=0.7 $\$\cdot m^{-3}$.

6 Conclusions

This work addressed the optimization of dual-purpose desalination plants (DPDP) – simultaneous production of electricity and freshwater – by integrating a combined-cycle heat and power (CCHP) plant with a multiple stage flash (MSF) desalination process.

Mathematical programming techniques and a generalized gradient-based optimization algorithm were used. A superstructure-based representation of the heat recovery steam generator (HRSG) of the CCHP was proposed and a mixed-integer nonlinear programming (MINLP) model was derived from it. The superstructure and the model embedded simultaneously several attractive candidate structures, from single-pressure (1P) to triple-pressure (3P) HRSG configurations. Series, parallel and series-parallel heat exchanger arrangements as well as steam reheating were allowed.

The existing Shuaiba North DPDP (1P-HRSG), located in Kuwait, was used as a reference case for model validation and investigate optimized revamping cases.

In a first optimal revamping problem, the freshwater production rate per unit of total heat transfer area required in the HRSG ($\dot{D}$ / $THTA_{HRSG}$ ratio) was maximized, keeping the same MSF desalination system (heat transfer areas and dimensions of the flashing stages) and gas turbine (flue-gas flowrate and temperature entering the HRSG) as in the reference case. Interestingly, an extra amount of 13.782 kg/s of freshwater was produced when the 1P-HRSG in the Shuaiba North plant was replaced with a 3P-HRSG with a significant reduction in the $THTA_{HRSG}$ of 19.2%.

A second optimal revamping problem considered the possibility to sell electricity and freshwater. In this case, the profit – defined as the difference between the revenue for selling electricity and freshwater and the total cost of the integrated system – was maximized. The sale prices for which it is economically convenient to generate extra electricity and freshwater were determined. When a 3P-HRSG replaced the original 1P-HRSG in the Shuaiba North plant, higher profit values were achieved. The differences in profit increased with increasing sale prices, ranging between 1.991×10^{-6} $\$\cdot yr.^{-1}$ for sale prices of electricity and freshwater of 0.05 $\$\cdot kWh^{-1}$ and $P_{s,WAT}$=1.2 $\$\cdot kWh^{-1}$, respectively, and 13.735×10^{-6} $\$\cdot yr.^{-1}$ for sale prices of 0.5 $\$\cdot kWh^{-1}$ and 1.5 $\$\cdot m^{-3}$, respectively.

References

[1] Baccioli A, Antonelli M, Desideri U, Grossi A. Thermodynamic and economic analysis of the integration of Organic Rankine Cycle and Multi-Effect Distillation in waste-heat recovery applications. Energy 2018; 161: 456–469. https://doi.org/10.1016/j.energy.2018.07.150

[2] You H, Hang J, Liu Y. Performance assessment of a CCHP and multi-effect desalination system based on GT/ORC with inlet air precooling. Energy 2019; 185: 286–298. https://doi.org/10.1016/j.energy.2019.06.177

[3] Alharbi S, Elsayed ML, Chowa LC. Exergoeconomic analysis and optimization of an integrated

system of supercritical CO2 Brayton cycle and multi-effect desalination. Energy 2020; 197: 117225. https://doi.org/10.1016/j.energy.2020.117225

[4] Kouta A, Al-Sulaiman FA, Atif M. Energy analysis of a solar driven cogeneration system using supercritical CO2 power cycle and MEE-TVC desalination system. Energy 2017; 119: 996–1009. https://doi.org/10.1016/j.energy.2016.11.041

[5] Luo C, Zhang N, Lin H. Proposal and analysis of a dual-purpose system integrating a chemically recuperated gas turbine cycle with thermal seawater desalination. Energy 2011; 36: 3791–3803. https://doi.org/10.1016/j.energy.2010.11.029

[6] Gadhamshetty V, Gude VG, Nirmalakhandan N. Thermal energy storage system for energy conservation and water desalination in power plants. Energy 2014; 66: 938–949. https://doi.org/10.1016/j.energy.2014.01.046

[7] Hamed OA, Al-Washmi HA, Al-Otaibi HA. Thermoeconomic analysis of a power/water cogeneration plant. Energy 2006; 31: 2699–2709. https://doi.org/10.1016/j.energy.2005.12.011

[8] Rensonnet T, Uche J, Serra L. Simulation and thermoeconomic analysis of different configurations of gas turbine (GT)-based dual-purpose power and desalination plants (DPPDP) and hybrid plants (HP). Energy 2007; 32: 1012–1023. https://doi.org/10.1016/j.energy.2006.10.015

[9] Ahmadi P, Khanmohammadi S, Musharavati F, Afrand M. Development, evaluation, and multi-objective optimization of a multi-effect desalination unit integrated with a gas turbine plant. Applied Thermal Engineering 2020; 176: 115414. https://doi.org/10.1016/j.applthermaleng.2020.115414

[10] Wu L, Hu Y, Gao C. Optimum design of cogeneration for power and desalination to satisfy the demand of water and power. Desalination 2013; 324: 111–117. https://doi.org/10.1016/j.desal.2013.06.006

[11] Shakib SE, Amidpour M, Aghanajafi C. Simulation and optimization of multi effect desalination coupled to a gas-turbine plant with HRSG consideration. Desalination 2012; 285: 366–376. https://doi.org/10.1016/j.desal.2011.10.028

[12] Valero A, Serra L, Lozano MA. Structural theory of thermoeconomics. International symposium on thermodynamics and the design, analysis and improvement of energy systems, New Orleans, ASME Book No. H00874, 1993. pp. 189-198.

[13] Lozano MA, Valero A. Theory of the exergetic cost. Energy 1993; 18: 939–960. https://doi.org/10.1016/0360-5442(93)90006-Y

[14] Guan J, Aral MM, Progressive genetic algorithm for solution of optimization problems with nonlinear equality and inequality constraints. Applied Mathematical Modelling 1999; 23: 329–343. https://doi.org/10.1016/S0307-904X(98)10082-3

[15] Mussati SF, Aguirre PA, Scenna NJ. Novel Configuration for a Multi Stage Flash-Mixer Desalination System. Industrial and Engineering Chemistry Research 2003; 42: 4828–4839. http://pubs.acs.org/doi/pdf/10.1021/ie020318v

[16] Mussati SF, Cignitti S, Mansouri SS, Gernaey KV, Morosuk T, Mussati MC. Configuration

optimization of series flow double-effect water-lithium bromide absorption refrigeration systems by cost minimization. Energy Conservation and Management 2018; 158: 359–372. https://doi.org/10.1016/j.enconman.2017.12.079

[17] Arias AM, Mussati MC, Mores PL, Scenna NJ, Caballero JA, Mussati SF. Optimization of multi-stage membrane systems for CO2 capture from flue gas. International Journal of Greenhouse Gas Control 2016; 53: 371–390. https://doi.org/10.1016/j.ijggc.2016.08.005

[18] Mussati SF, Barttfeld M, Aguirre PA, Scenna NJ. A disjunctive programming model for superstructure optimization of power and desalting plants. Desalination 2008; 222: 457–465. https://doi.org/10.1016/j.desal.2007.01.162

[19] Mussati SF, Aguirre PA, Scenna NJ. Dual Purpose Desalination Plants. Part II. Optimal Configuration. Desalination 2003; 153: 185-189. https://doi.org/10.1016/S0011-9164(02)01126-8

[20] Zak GM. Thermal desalination: structural optimization and integration in clean power and water Zak, Gina Marie Thesis (S.M.). Massachusetts Institute of Technology, Dept. of Mechanical Engineering, 2012.

[21] Martelli E, Elsido C, Mian A, Maréchal F. MINLP model and two-stage algorithm for the simultaneous synthesis of heat exchanger networks, utility systems and heat recovery cycles. Comp Chem Eng 2017;106:663–689. http://dx.doi.org/10.1016/j.compchemeng.2017.01.043.

[22] Manassaldi JI, Arias AM, Scenna NJ, Mussati MC, Mussati SF. A discrete and continuous mathematical model for the optimal synthesis and design of dual pressure heat recovery steam generators coupled to two steam turbines. Energy 2016; 103: 807–823. https://doi.org/10.1016/j.energy.2016.02.129

[23] Manassaldi JI, Mussati MC, Scenna NJ, Mussati SF. Development of extrinsic functions for optimal synthesis and design—Application to distillation-based separation processes. Computers and Chemical Engineering 2019; 125: 532–544. https://doi.org/10.1016/j.compchemeng.2019.03.028

[24] Abu-Zahra MRM, Niederer JPM, Feron PHM, Versteeg GF. CO2 capture from power plants: Part II. A parametric study of the economical performance based on mono-ethanolamine. Int. J. Greenh. Gas Control 2007; 1: 135–142. https://doi.org/10.1016/S1750-5836(07)00032-1

[25] Rao AB, Rubin ES. A Technical, Economic, and Environmental Assessment of Amine-Based CO2 Capture Technology for Power Plant Greenhouse Gas Control. Environ. Sci. Technol. 2002; 36: 4467–4475. https://doi.org/10.1021/es0158861

[26] Binamer A, Darwish A. Cost allocation in cogeneration power-desalination plant utilising gas/steam combined-cycle (GTCC) in Kuwait. International Journal of Exergy 2014; 14: 275–302. doi:10.1504/IJEX.2014.061029